Computers & Geosciences 89 (2016) 32–43

Contents lists available at ScienceDirect

Computers & Geosciences

journal homepage: www.elsevier.com/locate/cageo

Research paper

Precursors predicted by artificial neural networks for mass balance calculations: Quantifying hydrothermal alteration in volcanic rocks

Sylvain Trépanier [a,b], Lucie Mathieu [a], Réal Daigneault [c,*], Stéphane Faure [a]

[a] CONSOREM – Mineral Exploration Research Consortium, 555 Boulevard de l'Université, Chicoutimi, Canada, G7H 2B1
[b] Redevance Aurifères Osisko Ltd., Exploration Osisko Baie James – 300 rue Saint-Paul (Office 200), Québec, Québec, Canada G1K 7R1
[c] Centre d'études sur les Ressources Minérales (CERM) – Université du Québec à Chicoutimi, 555 Boulevard de l'Université, Chicoutimi, Canada, G7H 2B1

ARTICLE INFO

Article history:
Received 2 February 2015
Received in revised form
9 January 2016
Accepted 11 January 2016
Available online 12 January 2016

Keywords:
Hydrothermal alteration
Immobile elements
Mineral exploration
Neural networks
Multi-layer perceptron
Mass balance calculations

ABSTRACT

This study proposes an artificial neural networks-based method for predicting the unaltered (precursor) chemical compositions of hydrothermally altered volcanic rock. The method aims at predicting precursor's major components contents (SiO_2, FeO^T, MgO, CaO, Na_2O, and K_2O). The prediction is based on ratios of elements generally immobile during alteration processes; i.e. Zr, TiO_2, Al_2O_3, Y, Nb, Th, and Cr, which are provided as inputs to the neural networks. Multi-layer perceptron neural networks were trained on a large dataset of least-altered volcanic rock samples that document a wide range of volcanic rock types, tectonic settings and ages. The precursors thus predicted are then used to perform mass balance calculations. Various statistics were calculated to validate the predictions of precursors' major components, which indicate that, overall, the predictions are precise and accurate. For example, rank-based correlation coefficients were calculated to compare predicted and analysed values from a least-altered test dataset that had not been used to train the networks. Coefficients over 0.87 were obtained for all components, except for Na_2O (0.77), indicating that predictions for alkali might be less performant. Also, predictions are performant for most volcanic rock compositions, except for ultra-K rocks. The proposed method provides an easy and rapid solution to the often difficult task of determining appropriate volcanic precursor compositions to rocks modified by hydrothermal alteration. It is intended for large volcanic rock databases and is most useful, for example, to mineral exploration performed in complex or poorly known volcanic settings. The method is implemented as a simple C++ console program.

1. Introduction

Grassroots, or regional mineral exploration, necessitates the use of powerful and simple methods to interpret large amounts of chemical data. The interpretation and quantification of hydrothermal alterations in volcanic terrains, for instance, is particularly important as many economic substances are accumulated by the circulation of hydrothermal fluids in areas with magmatic activity, and because altered rocks are one of the main vectors used to explore for such mineralisations.

Geochemical studies of hydrothermally altered rocks aim at determining the amount of elements gained and lost during alteration of an initially fresh rock (i.e. the precursor), by performing mass balance calculations while assuming that one or more elements is immobile during alteration (see Gresens (1967)). Gresens' (1967) approach has been extensively and successfully used (MacLean and Kranidiotis, 1987; Shriver and MacLean, 1993; Cadieux et al., 2006; to name a few).

A major question that arises when using such mass balance equations concerns the choice of an appropriate precursor for the studied altered sample. Precursor's compositions are usually obtained by analysing "fresh" samples (i.e. samples that lack alteration minerals) that have been geologically related to the altered sample using detailed knowledge of the local geology (e.g. Grant, 1986, 2005). Such approaches are possible only for detailed deposit-scale studies, if fresh rocks exist and if our level of knowledge of the area render their identification possible. Even so, usually nothing proves that the fresh sample is an exact match for the precursor to the altered sample, and these difficulties can make mass balance calculations un-reliable.

At a more regional scale, on the other hand, these difficulties can be in-surmountable. Thus, orebody targeting using chemical datasets more often rely on alteration indexes (ratio of major elements), which values are sensitive to the precursor's compositions and could provide miss-leading indications on the intensity of alteration (see discussion in Trépanier et al. (2015)).

* Corresponding author.
E-mail address: real_daigneault@uqac.ca (R. Daigneault).

http://dx.doi.org/10.1016/j.cageo.2016.01.003
0098-3004/

Mass balance calculations would be more reliable if a suitable precursor composition to an altered rock could be determined directly from the chemical characteristics of the altered sample, thus providing a precursor adapted to this sample.

This paper proposes a method for estimating the composition in SiO_2, CaO, MgO, FeO^T, K_2O, and Na_2O of fresh precursors to altered volcanic rocks, using ratios of commonly analysed least mobile elements (i.e. Zr, TiO_2, Al_2O_3, Y, Nb, Th, and Cr) and a regression method (i.e. artificial neural network). The method is provided as supplemental material, as a simple C++ program that calculates precursor compositions (this study) prior performing mass balance calculations (using published methods).

2. Methodology

2.1. Description of the method

In this contribution, a method to predict fresh precursors from the chemical composition (i.e. immobile elements content) of altered volcanic rocks is presented. Predictions are performed for magmatic rocks only because relatively simple relationships, which are controlled by magmatic processes, exist between the trace and major elements content of such rocks. For example, Zr and Si are both incompatible elements that tend to increase during fractional crystallisation, making Zr a proxy for Si (see Winchester and Floyd (1977)).

Also, precursor predictions are performed using ratio of elements considered immobile in regard of hydrothermal processes. Ratios are used because the value of immobile elements ratios is not modified by mass or volume changes and because ratios are unlikely to be strongly fractionated by hydrothermal processes. Instead, such ratios mostly vary between volcanic rocks of different types and affinities, which originate from various sources and different conditions of partial melting, fractional crystallisation and other processes. Because ratios of immobile elements are insensitive to alteration and can reflect geodynamic settings and differentiation, they have been extensively used by discrimination diagrams (e.g. Winchester and Floyd, 1977; Barrett and MacLean, 1994), and their use is here extended to predict major elements compositions of the fresh precursors to altered volcanic rocks.

In order to relate immobile element ratios to the major elements of volcanic rocks, the typical composition of least-altered volcanic rocks is documented using a large dataset of samples of various volcanic rock types from different tectonic settings and ages (see Section 3.1; Figs. 1 and 2) and on which predictions are performed using a method able to solve regression problems. Since this prediction implies a large variety of rocks, non-linear solutions can be expected. Tests were initially performed with various methods, e.g. multiple regressions, but non produced results as good as these obtained with neural networks. For this reason, a multi-layer perceptron neural network was trained on a large dataset of least-altered volcanic rocks and used to predict precursor compositions.

2.2. Immobile elements ratios

Hydrothermal fluids modify the mineral assemblages (alteration) and chemical composition (metasomatism) of rocks, with various minerals and elements being more or less susceptible to be modified or displaced. Here, the immobile elements used by the proposed method are immobile in most mineralised contexts and are commonly analysed, so that the method can be applied to datasets typically used by exploration geologists.

Elements relatively immobile during hydrothermal alteration, weathering and low-grade metamorphic processes are characterized by ions that are of intermediate ionic potential (0.03–0.1 ppm^{-1}; Pearce, 1996). From the elements considered immobile by various authors (Cann, 1970; Pearce and Norry, 1979; Hill et al., 2000; Kurtz et al., 2000; Hastie et al., 2007), seven elements were selected as inputs to the neural networks (i.e. Zr, Al, Ti, Nb, Cr, Y, and Th) because, according to Pearce (1996), these elements are sufficient to properly characterize most basalts and, presumably, most volcanic rocks. These elements have indeed been used to characterize various magmatic processes, such as: (1) the degree of differentiation (Winchester and Floyd, 1977; Pearce and Norry, 1979); (2) the alkalinity of rocks (Pearce and Cann, 1973); (3) the geodynamic context

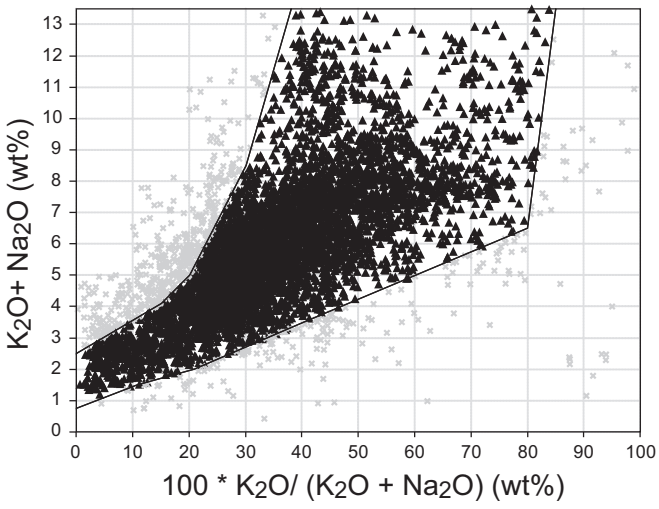

Fig. 1. Modified Hughes' diagram (Hughes, 1972) on which the Georoc dataset is represented. This diagram has been used to remove K–Na altered samples from the initial dataset. Black triangles highlight kept samples and grey crosses correspond to discarded samples.

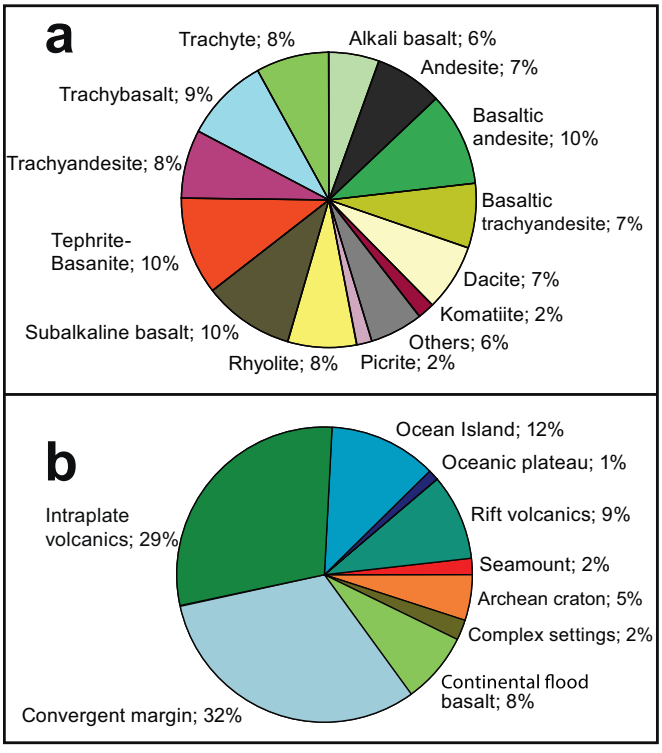

Fig. 2. Pie plots displaying several characteristics of the samples of the least-altered dataset ($n=5810$). The displayed characteristics are: (a) the proportions of rock types (see IUGS geochemical classification of volcanic rocks; Le Maitre et al. (1989)); and (b) the tectonic settings, as identified in the Georoc database.

(Pearce and Cann, 1973; Wood, 1980; Meschede, 1986; Schandl and Gorton, 2002; Hastie et al., 2007; Ross and Bédard, 2009); (4) the depth of partial melting and/or the composition of the source (Drummond and Defantt, 1990; Petford and Atherton, 1996; Pearce, 2008); etc.

The selected immobile elements are considered relatively immobile in many, but not all, hydrothermal processes, as various parameters may increase the mobility of these elements (Hynes, 1980; McCulloch and Gamble, 1991; Pearce, 1996; Hill et al., 2000). For example, the mobility of Zr, Y, Ti, and Nb has been documented from oceanic crust samples (Cann, 1970), in rocks altered by fluorine-enriched fluids (Salvi et al., 2000; Jiang et al., 2005) and in various mineralised areas (Finlow-Bates and Stumpfl, 1981; Van Dongen et al., 2010). However, Zr, Al, Ti, Nb, Cr, Y, and Th are considered to be sufficiently immobile in most cases; as such, the method developed here should be applicable to most mineralised contexts.

Even so, it is recommended to test for the immobility of Zr, Al, Ti, Nb, Cr, Y, and Th prior performing the precursors' prediction described below, by using, for example, binary plots (see Cann (1970)) or Pearce Element Ratio diagrams (Pearce, 1968; Stanley and Russell, 1989) adapted to the study of hydrothermal processes (Stanley and Madeisky, 1994). Also, in certain well constrained contexts, it might be possible to sample a fresh precursor and the immobility of elements could be verified using the isocon diagram of Grant (1986, 2005). Study of element's variabilities could also be performed (Schiano et al., 1993).

2.3. Artificial neural networks definition

Artificial neural networks are numerical models made of simple processing elements named neurons (Zurada, 1992). Neurons are interconnected by links, to which values (i.e. weights) are attributed. Weights describe the strength of the connections between neurons. Neural networks are adaptive; i.e. "knowledge" is gained through a process of training and learning from examples. After training, the "knowledge" is stored by the weight values. Also, the learning process can be supervised, if the input examples already contain the desired outputs.

Many neural network topologies exist. Here, multilayer perceptrons (MLP) are supervised networks that were selected because of their capacity to approximate nearly any function (Hornik et al., 1989). The first layer, called the input layer, distributes the input data (i.e. chemical analyses of volcanic rocks in our case) to the network. The MLP's input layer is made of several neurons, i.e. one for each input variable. Processing (i.e. additions, multiplications and other non-linear transformations; Fig. 3) is performed by one or more hidden layers of neurons. The final, predicted results, is calculated by the output layer, which contains an amount of neurons that is dependent on the number of target values to be modelled by the network.

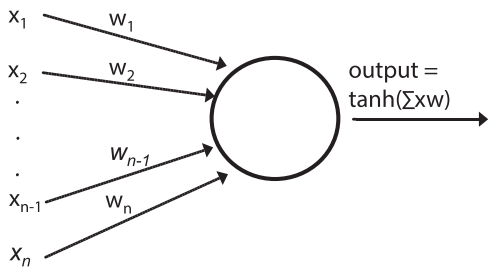

Fig. 3. Sketch showing calculations performed at an individual neuron within a multilayer perceptron (MLP) network. The neuron's input is calculated by multiplying the input signal (x_i) by the weight of the links (w_i). Inputs are summed and then transformed by a non-linear function, in this case the hyperbolic tangent function. The result corresponds to neuron's output.

An MLP is trained using successive cycles. During each cycle, training examples are fed to the network, which gradually modifies the weights in order to diminish the sum of the squared error between desired (actual) and output (modelled) values. The network's predictions thus improve at each cycle but excessive learning can lead to overfitting, which should be avoided as an overfitted network has started to learn the noise, or random component, of the input dataset and cannot be generalised. To avoid overfitting and to evaluate the performance of a network, examples are often randomly separated into three subsets: (1) the *training set*; (2) the *cross-validation set*; and (3) the *test set*.

The *training set* is used to train the network. The *cross-validation set* is used to monitor the sum of squared errors between the desired and modelled outputs and to avoid overfitting (see early stopping procedure; Wang et al. (1994)). The *test set*, on the other hand, is used to evaluate the generalisation performance of the network once the training is completed. In addition, networks are usually trained several times using random initial network weights to avoid local minima in the approximated function.

3. Data processing

3.1. Least-altered volcanic rocks dataset

Relationships between major and immobile elements are evaluated here with neural networks using a large chemical dataset of modern volcanic rocks from around the World. Post-Archean to modern rocks are used because they are well constrained samples for which names, geodynamic settings and freshness can be confidently established; i.e. characteristics that would be harder to determine for more ancient samples. Besides, there might be large differences between ancient (Archean) and modern geodynamics and bulk chemistry of magmas (e.g. Bédard, 2006), but this does not necessarily mean that the relationships between major and immobile elements, in magmas, changed between the Archean and more recent times; i.e. if it is considered that partial melting, fractional crystallisation and other processes operate in similar ways at all times. Also, volcanic rocks are used because a large dataset is needed, and because the highest quality and largest dataset of magmatic rocks available, i.e. the Georoc web database (Sarbas, 2008; GEOROC, 2011), documents mostly volcanic rocks.

The Georoc dataset was thus used and processed as follows. First, all volcanic samples from the "Precompiled Files – > Rocks" page were downloaded; i.e. a total of 110,724 samples of volcanic rocks. Then, the following criteria were used to filter the dataset.

1. Only samples with major elements, LOI, Zr, Cr, Nb, Y, and Th analysed were retained.
2. Only samples with Nb $\geq$ 8 ppm, or with Nb $<$ 8 ppm but precise to the tenth decimal place, were kept.
3. Samples described as altered in the Georoc dataset were rejected (see codes M, E, T; GEOROC, 2011).
4. Samples (picrites, komatiites, meimechites, and boninites excepted) with LOI $>$ 2.5% (i.e. approximately $H_2O^+ > 2\%$ and $CO_2 > 0.5\%$ that characterises most altered volcanic rocks according to the IUGS volcanic rock classification; Le Maitre et al., 1989) were rejected.
5. Samples (picrites, picrobasalts, komatiites, meimechites, and boninites excepted) plotting outside the "fresh field" of a modified Hughes (1972) diagram (i.e. diagram with a "fresh field" expanded toward the right to include fresh ultra-K rocks) were rejected (Fig. 1).
6. Samples with a Chemical Index of Alteration (CIA; Nesbitt, 2003) over 52.5 (i.e. 52.5 was used instead of 50 to retain slightly peraluminous igneous rocks) were discarded.

7. To ensure that a single oversampled volcanic unit is not over-represented in the dataset, a maximum of 25 samples per publications has been conserved, using random subsampling.
8. The Georoc dataset is also strongly skewed toward basalts, basaltic andesites, and to a lesser extent, andesites. For neural networks processing, more balanced inputs are preferable. The dataset was thus subsampled to ensure that no single rock type (as defined by IUGS; Le Maitre et al., 1989) represents over 10% of the final dataset. Note that these rock types, or groups, are no longer used hereafter, as the methodology is applied across a continuum of compositions.

The final dataset, considered to represent fresh rocks, contains 5810 samples (Fig. 2a) from various tectonic settings (Fig. 2b).

3.2. Artificial neural networks processing

The Georoc database's samples have then been used to train multi-layers supervised networks (i.e. MPL, see Section 2.3). Prior performing the training, the dataset was randomly split into three subsets: (1) the *training set*, to which 2905 samples (50%) were allocated; (2) the *cross-validation set* received 1453 samples (25%); and (3) the *test set* received the remaining 1452 samples (25%). Also, tests were performed using transformed data (centred log-ratios) and un-transformed, compositional, data. As both tests produced similar results (see Section 5.1), only un-transformed data were retained.

The inputs fed to the MLP are ratios of immobile elements and outputs (i.e. the components to be predicted) are major mobile elements. Before processing, the chemical analyses were re-calculated on a LOI-free basis and input chemical elements were normalised. Once normalised, the values of each variable is comprised between 0 and 1 and, as such, the units of input data (wt% or ppm) is unimportant.

Then, the neural networks were trained using the Levensberg–Marquardt supervised algorithm (NeuroSolutions 6.11 for excel software; NeuroDimension, 2012). The MLP networks used here contain an input layer made of 21 neurons (i.e. number of possible ratios between the immobile elements), one hidden layer and uses an hyperbolic tangent transfer function. To determine the optimal number of hidden neurons for the hidden layer of each network, five models that contain 2, 4, 6, 8, and 10 hidden neurons, respectively, were tested. Each test consisted in 3 runs, or trainings, of the networks and the most performant network (i.e. network with minimum sum of squared errors on the cross-validation set of all variations and runs) was kept (see Table 1).

Also, for each of the output components that are to be predicted (i.e. SiO_2, CaO, FeO^T, MgO, K_2O, Na_2O, Zr, and TiO_2), separate networks were trained. Note that the predicted Zr and TiO_2 values are used later, to perform mass balance calculations. Once trained with the *training* and cross-*validation sets*, and validated using the *test set* (see Section 5), the networks were used to predict precursor's compositions for new samples, and these precursors were used to perform mass balance calculations (see Section 4).

Eventually and to evaluate new samples (see Sections 6 and 7), an additional constrain was added to the model. It should be noted that trained neural networks provide valid predictions of precursor's compositions if and only if all the ratios of immobile elements of a sample to be evaluated are within the ranges of the *training set's* ratios. On the other hand, if the ratios of a sample fall outside the range of values of the *training set*, the prediction would be invalid and it should not be attempted. Similarly, the predicted values are expected to fall within the range of the *training set's* values, otherwise the prediction should be regarded as invalid. Valid ranges for immobile elements ratios and for predicted values were recorded from the networks and embedded in the software (see Section 4), in order to filter unsuitable samples and invalid outputs.

Table 1
Optimal number of hidden neurons contained in the hidden layer of neural networks.

Component	Optimal number of neurons
SiO_2	6
FeO^T	6
MgO	4
CaO	4
Na_2O	4
K_2O	4
TiO_2	2
Zr	6

4. Description of the software

4.1. Software

This study aims at modelling the chemical composition of fresh precursors to altered rocks, in order to facilitate mass balance calculations. The outputs of the neural networks (i.e. the results of the training process) can however be difficult to use as such, as the software used to train the neural networks (NeuroDimension, 2012) provides outputs files with a ".NSW" extension, which are simple ASCII text files that record the network's structure, parameters and weights.

To facilitate access to these results, they were embedded in a C++ program that is able to receive chemical analyses from new samples (input), that predicts the precursors' compositions and that performs mass balance calculation (see Section 4.2). This program provides users with the results of these calculations; i.e. precursors' compositions as well as mass changes values, which are provided in percent (relative mass change) and grams (absolute mass change).

4.2. Mass balance calculations

Once precursor values are predicted, mass balances can be calculated using the equation of Grant (1986, 2005), which is a rewritten form of Gresens' (1967) equation. Grant's (1986) equation defines a line called the "isocon" that passes through the origin of a multi-components graphic. The slope of the isocon yields the overall mass change between the fresh and altered sample, and this slope is constrained using elements immobile during the alteration process. Here, the slope value is obtained from the average of the slopes (Leitch and Lentz, 1994) calculated from TiO_2 and Zr (see Eq. (1)). Absolute mass changes, in grams, are then calculated for 100 g of precursor (see Eq. (2)) and relative mass changes are calculated in percent (see Eq. (3)).

$$M^P/M^A = \left(C^A_{TiO_2}/C^P_{TiO_2} + C^A_{Zr}/C^P_{Zr}\right)/2 \quad (1)$$

where C_{TiO_2} is the concentration of TiO_2; C_{Zr} is the concentration of Zr; "A" refers to the altered rock and "P" to the precursor rock as calculated by the neural networks. M^P and M^A are the equivalent masses before and after alteration. M^P/M^A is the slope of the isocon used in subsequent mass balance calculations.

$$\Delta C_i = C^A_i * M^A/M^P - C^P_i \quad (2)$$

$$\Delta C_i/C_i^P = 100*\left(M^A/M^P\right)\left(C_i^A/C_i^P\right) - 1 \quad (3)$$

where C_i is the concentration of element "i"; M^A/M^P is the inverse of the slope of the isocon calculated using Eq. (3); ΔC_i is the change in concentration of element "i" in grams per 100 g of precursor.

5. Neural network validations

Prior to using the method to predict new sample's precursors, the neural networks' outputs were validated. The consequences that Zr, Y, Nb, Cr, Th, Al, and Ti mobility might have on the prediction's accuracy are also tested. Overall, the proposed approach appears accurate, precise, and may tolerate a limited mobility of the immobile elements used by the model.

5.1. Evaluation of prediction's accuracy and precision

Once the training was completed, the accuracy and precision of the predictions were evaluated by feeding the *test set* to the trained networks and by comparing the predicted and actual values, using median errors (for accuracy) as well as, for precision, rank-based correlation coefficients, standard deviation of errors and normalised mean square error values (NMSE; Neurodimension, 2012) (see Eqs. (4) and (5).

$$MSE = \sum^N (\text{Actual value} - \text{Predicted value})^2 \quad (4)$$

$$NMSE = MSE/\text{Variance of the actual values} \quad (5)$$

where N is the number of samples in the training set, *MSE* is the mean square error, and *NMSE* is the normalised mean square error.

First, the *training set* was fed to the networks and the outputs were compared to the analysed values using scatter plots (Fig. 4). Overall, the points on the scatterplots tend to lie equally on either side of the 1:1 lines for the entire ranges of values, indicating that the prediction method is accurate and precise, in particular for TiO_2 and Zr, but less so for K_2O and Na_2O. Also, the model appears generally less precise for high values than for average or low values, especially for the predictions of Na_2O, Zr, TiO_2, and MgO (Fig. 4).

Then, median errors between predicted and analysed values were examined and found to be near 0 for all components and for both subalkaline and alkaline rocks (i.e. models are accurate) (Table 2). Standard deviation of error values are also low (Table 2), indicating that the method is precise (Table 2).

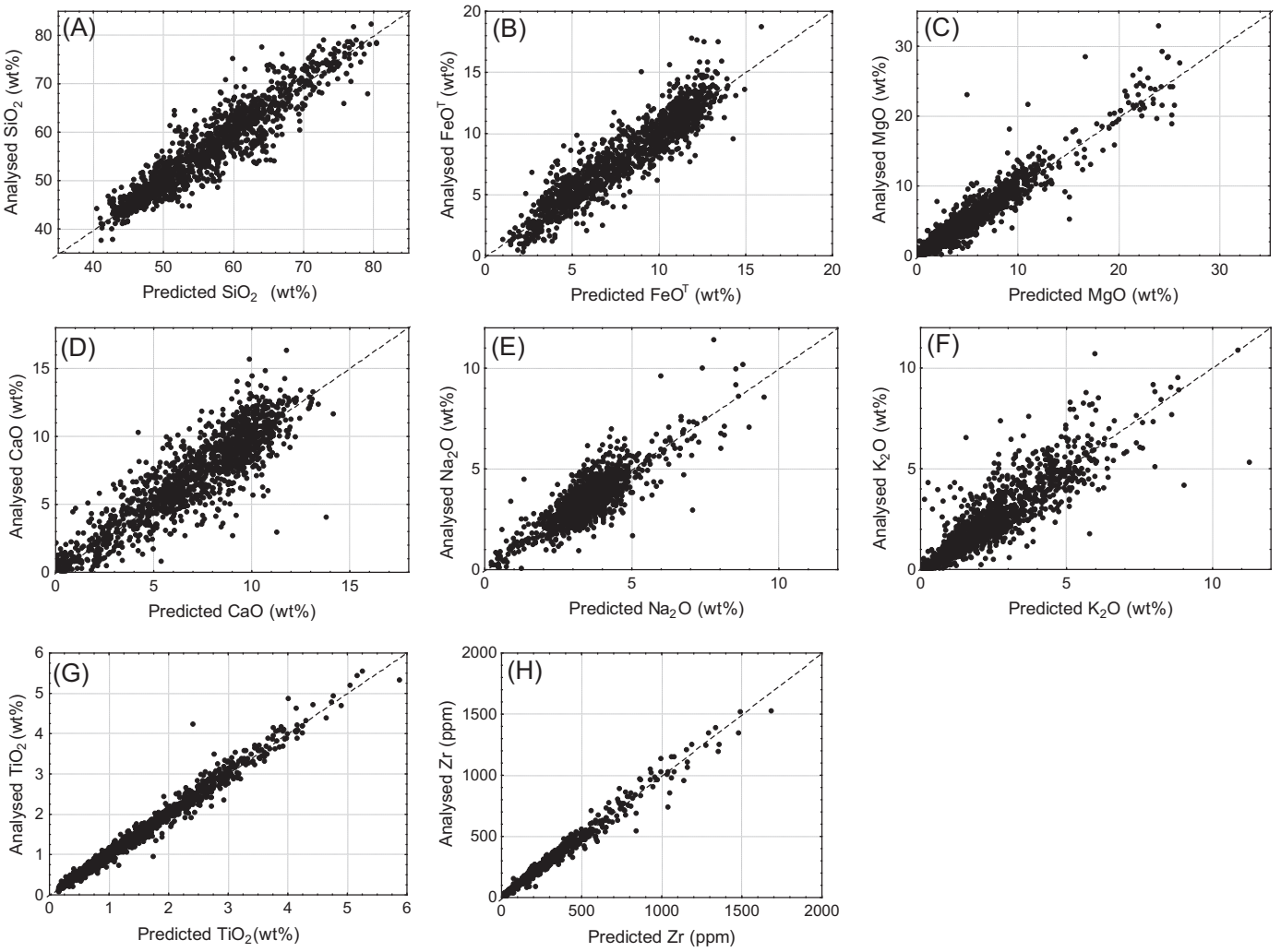

Fig. 4. Binary scatterplots of predicted vs analysed values, for the *test set* ($n=1452$). The 1:1 line is shown as dotted lines. The plots are available for the following elements: (a) SiO_2; (b) FeO^T; (c) MgO; (d) CaO; (e) Na_2O; (f) K_2O; (g) TiO_2; and (h) Zr.

Table 2
Median errors (ME), rank-based correlation coefficients (r), standard deviation of errors (SD) and normalised mean square errors (NMSE) for values predicted from the *test set*.

	Global				Alkaline rocks				Subalkaline rocks			
Component	ME	r	NMSE	SD	ME	r	NMSE	SD	ME	r	NMSE	SD
SiO_2	0.095	0.935	0.139	3.091	0.793	0.918	0.163	2.817	−0.415	0.931	0.158	3.092
FeO^T	0.056	0.935	0.150	1.224	−0.173	0.913	0.149	1.157	0.224	0.937	0.167	1.258
MgO	0.015	0.946	0.103	1.472	−0.025	0.945	0.128	1.207	0.036	0.925	0.096	1.644
CaO	−0.021	0.878	0.231	1.474	−0.147	0.803	0.248	1.544	0.041	0.891	0.234	1.413
Na_2O	0.007	0.767	0.378	0.674	−0.064	0.726	0.415	0.725	0.057	0.798	0.375	0.598
K_2O	0.109	0.891	0.269	0.838	−0.044	0.838	0.337	0.996	0.213	0.921	0.220	0.651
TiO_2	0.000	0.992	0.018	0.129	−0.027	0.992	0.021	0.148	0.013	0.986	0.030	0.109
Zr	2.271	0.989	0.022	30.22	−0.460	0.989	0.026	35.09	3.438	0.984	0.022	24.92

Median errors and correlations are calculated for the whole *test set* ($n=1452$), as well as for the following subsets: (1) subalkaline rocks ($n=833$); and (2) alkaline rocks ($n=619$). Alkalinity is determined using the TAS diagram (Le Bas et al., 1986).

Then, global rank-based correlation coefficients between predicted and analysed values were calculated (Table 2). Global correlations are over 0.93 for most components (i.e. the predictions are precise), except for Na_2O (0.77) and CaO (0.88), and are especially elevated for TiO_2 and Zr (0.99). Isocon evaluations, which are based on TiO_2 and Zr values, are thus likely to be precise (see Section 4.2). Also, note that correlations are generally slightly higher for subalkaline rocks than for alkaline rocks, with the maximum correlations' difference being 0.09 (for K_2O; Table 2).

Eventually, NMSE were calculated, which are found to be the lowest for TiO_2 and Zr, and the highest for Na_2O and K_2O (Table 2). NMSE values are also generally higher for alkaline rocks, except for FeO^T and TiO_2. Overall, the values of NMSE are generally low, validating the precision and accuracy of the models.

As mentioned in Section 3.2, the procedure described above uses un-transformed data but has also been performed using log-transformed data divided by the immobile element Al_2O_3. The rank-based correlation coefficients for both tests are similar except for SiO_2 (Table 3) and only the results of the test performed with un-transformed data were implemented by the C++ program provided as additional material to this contribution.

5.2. Effects of the mobility of an immobile element on major oxide predictions

Precursor compositions are predicted using ratios of elements considered immobile, but that might be mobile under certain conditions (see Section 2.2). In this section, the effect that such mobility might have on the precision and accuracy of predictions is modelled.

For each immobile element, one sample from the *test set*, for which the immobile element considered has approximately median value, was selected. The value of the considered immobile element of the selected samples was then increased and decreased by 33%, while the values of the other immobile elements were left untouched (Table 4); i.e. the ratios of immobile elements were modified. The resulting data were fed to the neural networks, which provided predictions reported in Table 4.

Table 3
Rank-based correlation coefficients (r) for values predicted from the whole *test set*, for tests using un-transformed data (see Table 2) and log-transformed data.

Un-transformed		Centred log-transformed	
Component	r	Component	r
SiO_2	0.935	$Ln(SiO_2/Al_2O_3)$	0.791
FeO^T	0.935	$Ln(FeO^T/Al_2O_3)$	0.941
MgO	0.946	$Ln(MgO/Al_2O_3)$	0.951
CaO	0.878	$Ln(CaO/Al_2O_3)$	0.914
Na_2O	0.767	$Ln(Na_2O/Al_2O_3)$	0.756
K_2O	0.891	$Ln(K_2O/Al_2O_3)$	0.880

This simple model of element's mobility indicates that moderate enrichments or depletions of Y, Cr, and Nb do not significantly modify the predicted values. Changes in Zr and TiO_2 moderately affect the predictions for FeO^T, MgO, and CaO (Table 4). On the other hand, changes in Zr and TiO_2 strongly affect Zr and TiO_2 predictions, respectively. As these elements are used to evaluate the isocon (see Section 4.2), it is recommended to evaluate the extent of their mobility prior using the method presented here (see Section 2.2).

6. Method validation using case studies

In this section, several fresh volcanic rocks, which were not included in the Georoc database used to train the neural network, are used to validate the approach (see case studies 1–3). Then, altered rocks from several mineralised areas (i.e. volcanogenic massive sulphide, or VMS, and porphyry deposits) are compiled, their precursors compositions are predicted and mass balance calculations are performed (see case studies 4–6).

6.1. Validation using fresh volcanic rocks

Case study 1 – Unaltered dacite samples from the 2004–2006 and 1986 eruptions of Mount Saint-Helens, Washington, USA, were compiled from Pallister et al. (2008). The major elements composition of these samples was then predicted using the neural networks, which accurately predicts most components (Fig. 5), except for K_2O values, which are moderately overestimated by 0.6–0.8% (Fig. 5f), and SiO_2 values, which are underestimated by ~2% (Fig. 5a).

Case study 2 – Ten samples of unaltered mafic volcanic rocks (alkaline basalts and hawaiites) from the Heimaey volcanic centre, Iceland, were compiled from Mattsson and Oskarsson (2005). Their analysed and predicted values are shown in Fig. 6. The predictions are generally good but systematic errors are observed for some elements, such as CaO (errors up to 1.5%). Also, overestimations of 2%, 0.1% to 0.4% and 1.5% are observed for SiO_2, K_2O, and MgO. Conversely, underestimations of 0.05–0.15% and 0.2–1% are observed for TiO_2 and Na_2O values. Overall, these errors on the predictions are minor and the method reproduces satisfactorily the compositions in major elements of the input rocks.

Case study 3 – Nineteen samples of mildly to strongly alkaline volcanic rocks from the Middle Latin Valley volcanic field, Italy, were compiled from Boari et al. (2009). These samples are described as devoid of alteration minerals and are named melilite-bearing kamafugitic rocks, plagioclase leucitites and leucitites,

Table 4
Effects that ±33% gains and losses of various immobile elements has on the predicted values calculated for selected samples.

	Original values (wt% for Al_2O_3 and TiO_2 and ppm for others)								Predicted values (wt% or ppm)							
Sample	Al_2O_3	TiO_2	Zr	Cr	Y	Nb	Th	SiO_2	FeOT	MgO	CaO	Na_2O	K_2O	TiO_2	Zr	Note
	14.37	0.61	364	2	43	18	17	69.8	4.20	0.64	2.25	4.18	4.37	0.67	370	Initial value
S MB01-60A	14.37	0.61	364	2	43	**12**	17	68.6	4.10	0.68	2.26	4.42	4.24	0.67	373	−33% Nb
	14.37	0.61	364	2	43	**24**	17	69.7	4.31	0.61	2.24	4.16	4.64	0.67	374	+33% Nb
	16.47	0.91	192	5	13	17	8.1	58.9	4.87	1.70	5.04	4.51	3.18	1.02	208	Initial value
s TS/90/01	16.47	0.91	***126***	5	13	17	8.1	56.0	**5.72**	2.32	**6.22**	4.09	2.99	1.05	**142**	−33% Zr
	16.47	0.91	***255***	5	13	17	8.1	59.9	**4.35**	1.47	4.75	4.47	3.54	0.99	**260**	+33% Zr
	12.58	2.77	220	404	24	34	3.8	47.3	11.81	10.1	9.59	2.96	1.18	2.88	231	Initial value
s SA60	12.58	2.77	220	404	***16***	34	3.8	47.9	11.34	10.5	9.04	3.57	**1.94**	2.78	231	−33% Y
	12.58	2.77	220	404	***32***	34	3.8	46.8	12.03	9.64	10.28	2.68	0.98	2.89	231	+33% Y
	16.54	0.68	163	76	13	14	10	62.4	4.55	2.63	4.47	4.05	2.61	0.72	169	Initial value
s S10	16.54	0.68	163	***50***	13	14	10	62.4	4.52	2.38	4.47	4.13	2.68	0.72	171	−33% Cr
	16.54	0.68	163	***101***	13	14	10	62.4	4.58	2.85	4.47	3.99	2.55	0.71	167	+33% Cr
	15.72	1.07	244	154	23.4	13.3	11	58.5	6.66	4.69	6.70	3.56	2.81	1.08	249	Initial value
s OC93	15.72	***0.71***	244	154	23.4	13.3	11	63.0	**5.17**	**3.60**	**5.40**	3.72	3.17	**0.72**	244	−33% TiO_2
	15.72	***1.42***	244	154	23.4	13.3	11	56.1	**7.85**	5.29	**7.50**	3.41	2.51	**1.39**	249	+33% TiO_2

Modelled changes of elements' original values are in bold italics. Important prediction changes (> 10%) are in bold.

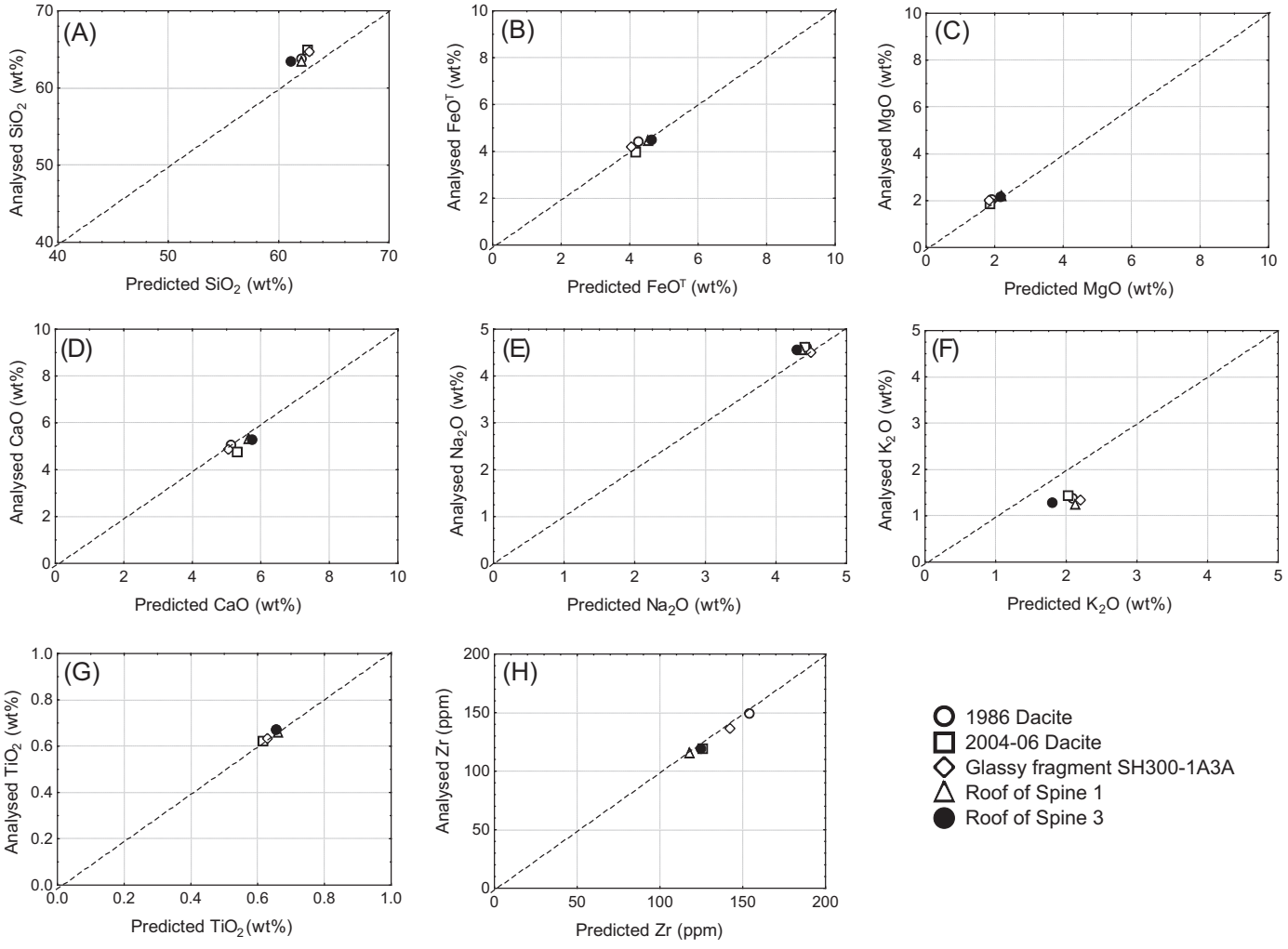

Fig. 5. Binary scatterplots of predicted vs analysed values, for samples from Mount Saint-Helens, USA (data from Pallister et al. (2008)). The 1:1 line is shown as dotted lines. The plots are available for the following elements: (a) SiO_2; (b) FeO^T; (c) MgO; (d) CaO; (e) Na_2O; (f) K_2O; (g) TiO_2; and (h) Zr.

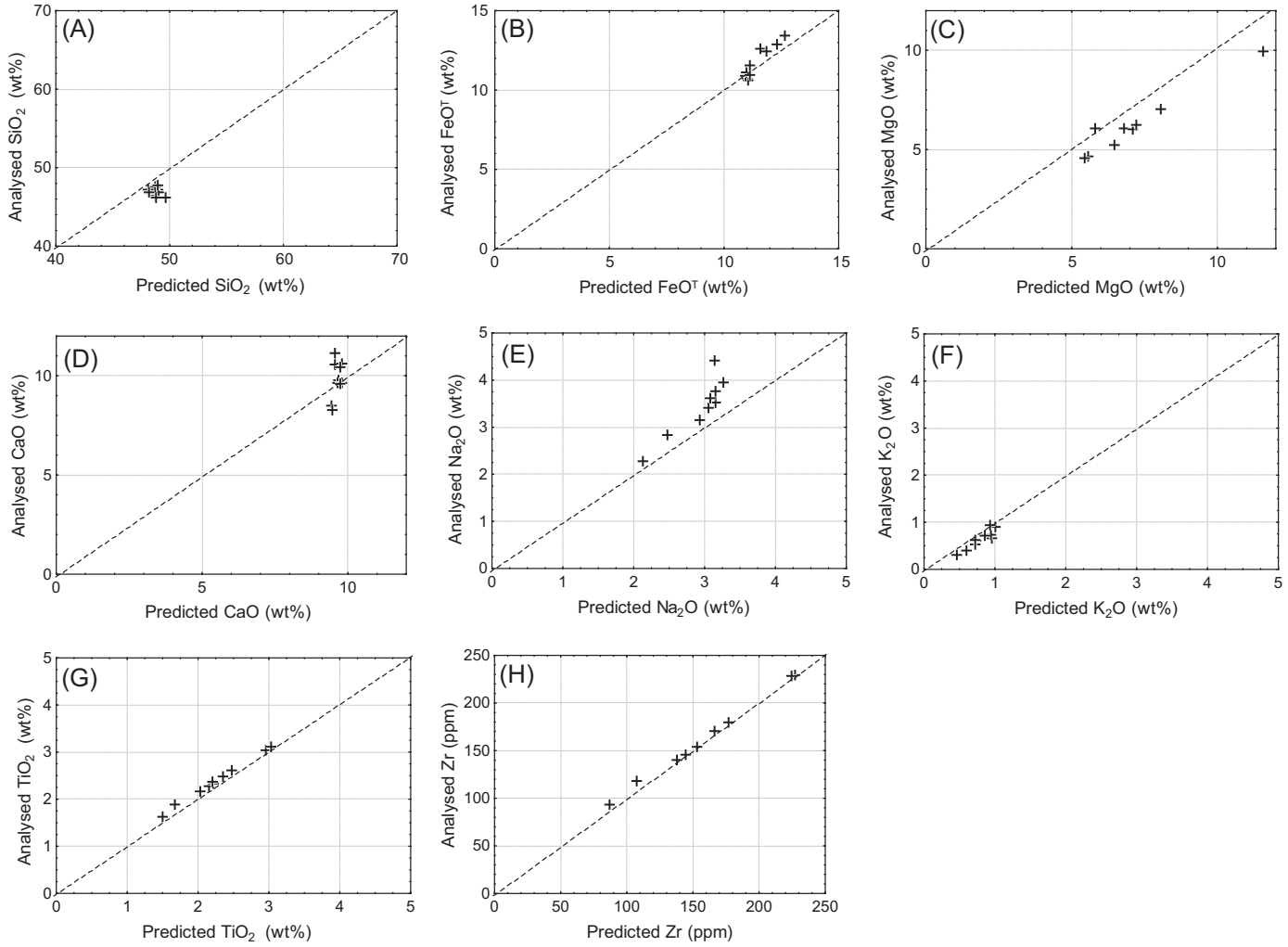

Fig. 6. Binary scatterplots of predicted vs analysed values, for samples from Heimaey volcanic zone, Iceland (data from Mattsson and Oskarsson (2005)). The 1:1 line is shown as dotted lines. The plots are available for the following elements: (a) SiO_2; (b) FeO^T; (c) MgO; (d) CaO; (e) Na_2O; (f) K_2O; (g) TiO_2; and (h) Zr.

shoshonites, and calc-alkaline rocks (Boari et al., 2009). Predicted values for these samples show that neural networks perform very poorly for nearly all components (except for Zr) (see Fig. 7), indicating that the method cannot be applied to ultra-K rocks. This is, however, a minor limitation as alkaline rocks in general, and ultra-K rocks in particular, represent small volumes of the crust.

6.2. Case study 4: Rhyodacite from the Phelps dodge VMS deposit

Twenty-two samples of altered rhyodacites from the Phelps Dodge VMS deposit, located in the Matagami Camp within the Archean Abitibi Greenstone Belt, in Québec, were compiled from MacLean and Kranidiotis (1987). These samples were selected because of their well-documented mass changes in Si, Mg, Fe, and other elements calculated by comparing each sample to the least altered, likely chloritised, sample #18 (see MacLean and Kranidiotis (1987)).

Major element contents of the 22 samples were predicted using the neural network solution. Also, mass balance calculations using the Grant's method (Grant, 1986), sample #18 as a fresh precursor and Al–Ti as immobile elements, were performed, following earlier similar calculations (see MacLean and Kranidiotis (1987) and Barrett and MacLean (1994)). Results of these calculations are displayed using a $Fe_2O_3^T$ + MgO vs SiO_2 diagram similar to this used by Barrett and MacLean (1994) (Fig. 8). On this diagram, the least-altered sample #18 is identified and the evolution of the alteration in three stages, as interpreted by MacLean and Kranidiotis (1987), is identified: (1) chloritisation (with Fe > Mg) and silicification; (2) silica leaching; and (3) destruction of Fe-chlorite (with residual Mg-chlorite) (Fig. 8).

Using the $Fe_2O_3^T$ + MgO vs SiO_2 diagram, we observe that mass changes calculated with a unique precursor (i.e. sample #18; Fig. 8a) are well reproduced by these calculated using precursors predicted by neural networks (Fig. 8b). Furthermore, neural network predictions confirm that sample #18 is altered (chloritized).

6.3. Case study 5: Neves Corvo VMS deposit

Twenty samples of altered felsic to intermediate volcanic rocks from the Neves Corvo VMS deposit, located in the Iberian pyrite belt, in Spain, were compiled from Relvas et al. (2006). The hydrothermal alteration is zoned, with a chlorite-enriched core enveloped by K-sericite and Na-sericite halos (Relvas et al., 2006). The method presented here was applied to samples from these three alteration zones and results are shown by Fig. 9.

The calculations confirm that the chlorite-enriched samples have gained Fe–Mg and lost alkali (see chloritisation). Also, the sericite-enriched samples have not gained Fe–Mg and have lost less alkali than the chloritized rocks; i.e. these rocks have mostly endure an acidic alteration, which is consistent with the acidic character of Neves Corvo deposit's hydrothermal fluids (see Relvas et al. (2006)). Thus, mass balance calculations enable a clear distinction between

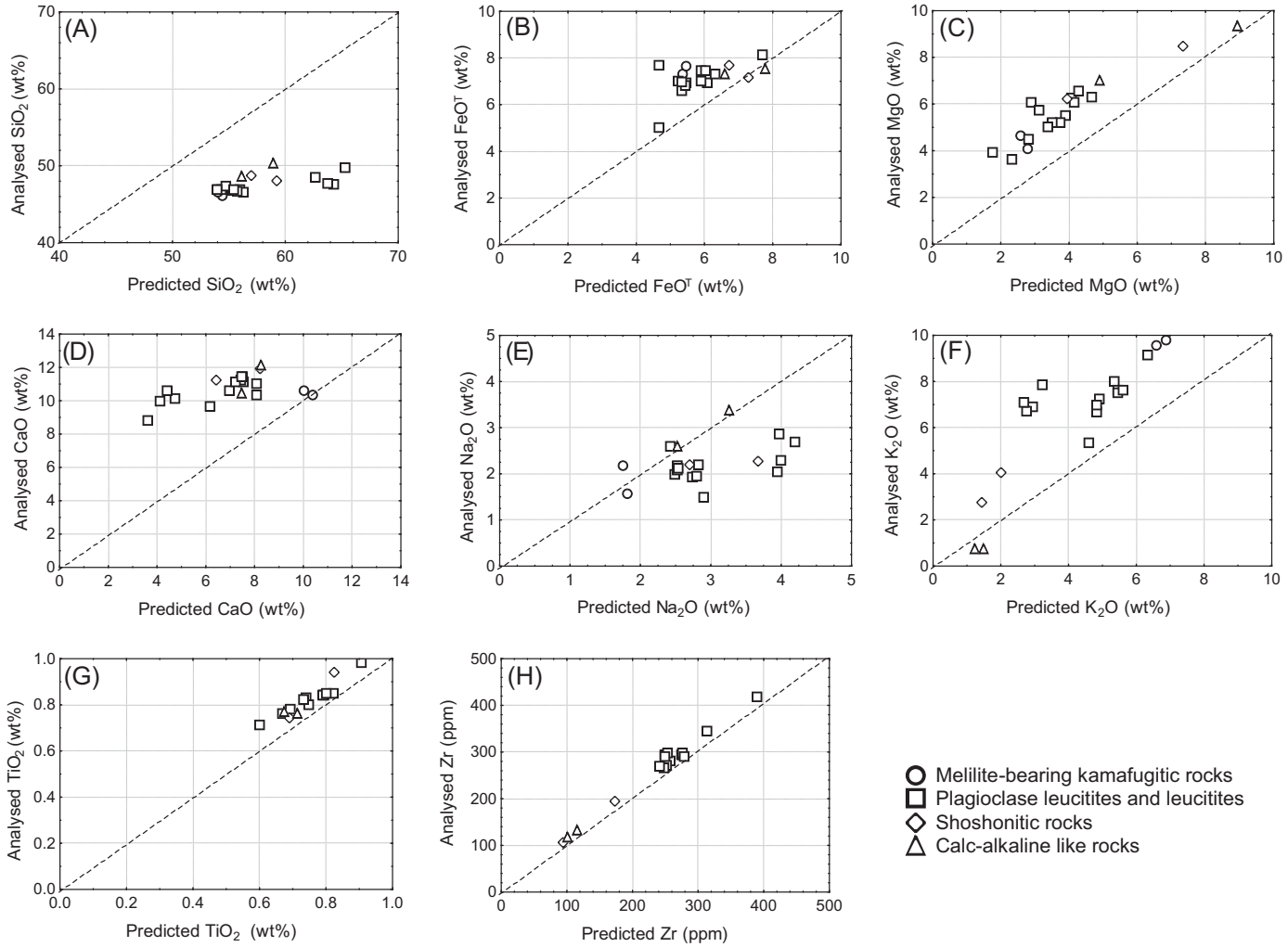

Fig. 7. Binary scatterplots of predicted vs analysed values, for samples from Middle Latin Valley, Roman Volcanic Province, Italy (data from Boari et al. (2009)). The 1:1 line is shown as dotted lines. The plots are available for the following elements: (a) SiO_2; (b) FeO^T; (c) MgO; (d) CaO; (e) Na_2O; (f) K_2O; (g) TiO_2; and (h) Zr.

sericitised and chloritised samples (see Fig. 9), pointing toward agreement between the calculation performed here and the petrology of the samples, as described by Relvas et al. (2006).

6.4. Case study 6: Porphyry deposits

A large amount ($n=565$) of samples of altered felsic to intermediate volcanic and intrusive rocks, collected in the vicinity of porphyry deposits, have been published by Dilles (2012) (see also Cohen (2011) and Cohen et al. (2011)). The petrology of alteration minerals contained in these samples has been studied in details, leading to their classification into the following groups: (1) albite; (2) albite, K-feldspar, sericite; (3) plagioclase; (4) plagioclase, K-feldspar; (5) sericite–albite; and (6) sericite (see Dilles (2012) and references included). Most of these alterations correspond to alkali gains (i.e. albitisation and K-feldspar alterations), locally accompanied by acidic alteration (i.e. sericitisation).

Neural networks calculations were performed on extrusive and intrusive rocks because, while the neural networks were trained using volcanic rocks only, there is no reason for the relationships between trace and major elements to be different in these two types of rocks. Predictions were thus obtained for all the compiled samples, prior calculating mass changes, and results are shown by Fig. 10. Calculations performed here indicate that albite- or plagioclase-enriched samples have gained Na (albitisation), that sericitised samples have gained K and lost Na, and that the other samples have gained variable amounts of Na and K (Fig. 10). Overall, a correlation is observed between the Na and K mass changes calculated here and petrographic observations of Dilles (2012).

7. Discussion and conclusions

This study proposes a method for predicting the composition in major elements of precursors to hydrothermally altered volcanic rocks, using artificial neural networks. To facilitate its utilisation by the reader, the method is embedded in a C++ console program that also performs mass balance calculations, allowing for the evaluation of alteration, in terms of type and magnitude, from large datasets of volcanic rocks.

Neural networks used here “learned” to predict the composition in major elements of volcanic rocks using ratios of immobile elements from a large dataset of fresh volcanic rocks compiled from the Georoc database. These predictions were checked for their accuracy and precision, which appear to be generally very good, except for uncommon volcanic rocks, i.e. ultra-K rocks (see Section 6.3), for which the method presented here should not be applied.

Also, evaluation of the precision of the method assumes that the dataset used to train the neural networks contains samples completely devoid of alteration. However, as alteration may initiate as early as during the cooling of a lava flow, it is reasonable to assume that the used dataset still contains slightly altered samples. As

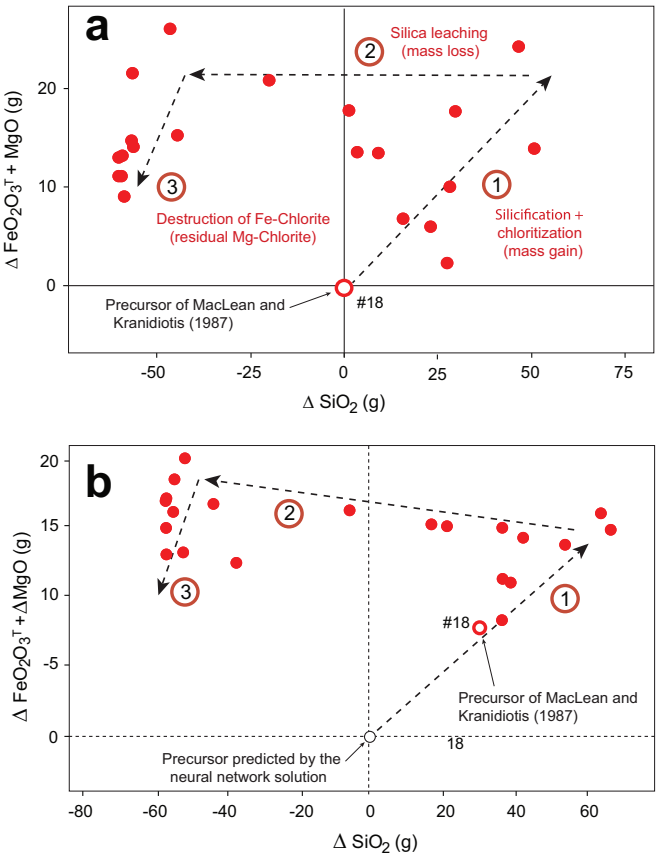

Fig. 8. Absolute mass changes, in grams, calculated for the rhyodacite rocks that host the Phelps Dodge deposits (samples from MacLean and Kranidiotis (1987)) and displayed in $Fe_2O_3^T + MgO$ vs SiO_2 diagrams inspired from Barrett and MacLean (1994). The mass changes have been calculated (a) using sample #18 as a fresh precursor (see MacLean and Kranidiotis (1987)); and (b) using precursors predicted by neural networks. Also, principal alteration paths are shown by arrows.

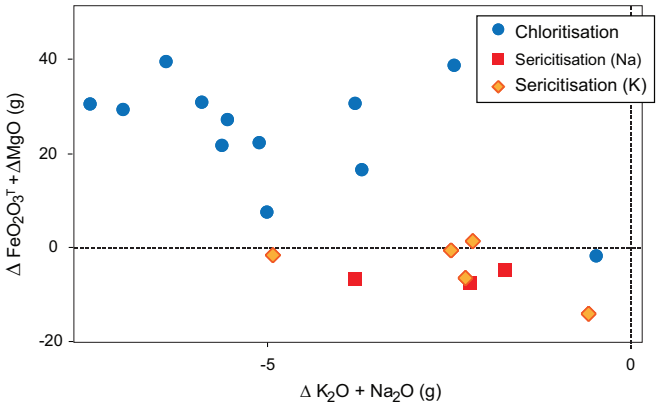

Fig. 9. Absolute mass changes, in grams, calculated for altered rocks from the Neves Corvo deposit (samples from Relvas et al. (2006)). The calculation was performed using neural networks and results are displayed in a $Fe_2O_3^T + MgO$ vs $K_2O + Na_2O$ diagram. Colour coding corresponds to alteration types, as interpreted by Relvas et al. (2006). (For interpretation of the references to color in this figure legend, the reader is referred to the web version of this article.)

alteration affects the most mobile elements, i.e. Na_2O, CaO, and K_2O, it may explain a part of the imprecision of the neural networks predictions. The rest of the imprecisions is likely inherited from the neural network inability to perfectly predict the proper precursor to every volcanic rock.

When the method is used on samples from mineralised areas, another source of inaccuracy of the predictions might arise, which

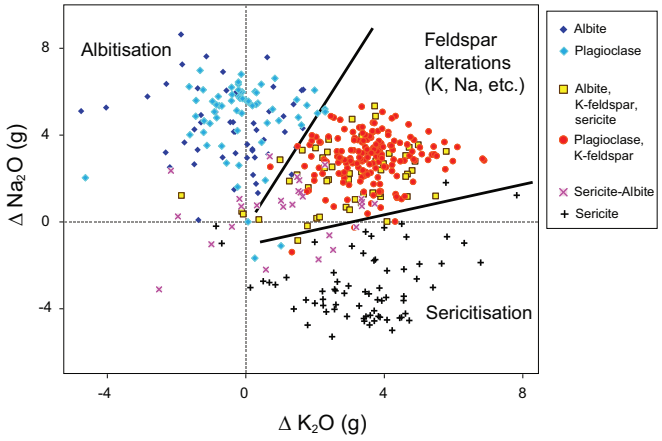

Fig. 10. Absolute mass changes, in grams, calculated for altered rocks from various northern American porphyry deposits (samples from Dilles (2012)). The calculation was performed using neural networks and results are displayed in a Na_2O vs K_2O diagram. Colour coding corresponds to alteration types, as interpreted by Dilles (2012) using detailed petrographic observations. (For interpretation of the references to color in this figure legend, the reader is referred to the web version of this article.)

is related to the mobility of the immobile elements used to constrain the model. To evaluate this problem, a "stress test" was performed (see Section 5.2), which shows that the predictions are robust and tolerate minor to moderate mobility of the immobile elements. However, if Zr and TiO_2 are mobile, the precursor prediction will be little affected, but the isocon will be erroneous, leading to inaccurate mass balance calculations. Note that, however, these elements are particularly immobile in most hydrothermal systems (e.g. Finlow-Bates and Stumpfl, 1981), except in particular settings (Jiang et al., 2005). As such, the method presented here should be operational in most contexts, but should be used with care in unusual areas, where there is reasons to doubt the immobility of Al, Cr, Y, Th, or Nb, and especially of Ti and Zr.

Also, the method was calibrated on a volcanic rocks dataset and should thus be applied to volcanic rocks only. However, chemical differences between extrusive and intrusive rocks are generally limited. In addition, there is no reason for the relationship between mobile and immobile elements to be different in both types of rocks. As such, the method should be applicable to magmatic rocks in general (see Section 6.4), as long as they are neither ultra-K rocks, nor rocks that do not have extrusive equivalents (i.e. cumulate and pegmatite). Note that the applicability of the method likely extends to metamorphic rocks with magmatic protoliths, as metamorphism does not modify the chemistry of rocks, except for volatiles. Thus, only sedimentary rocks and paragneisses should not be evaluated with this method.

In conclusion, the method presented here appears sufficiently precise and accurate to be used in most contexts to quantify alterations from altered magmatic rocks. It should be used on large datasets that document a large variety of volcanic units, when the volcanic stratigraphy is poorly constrained, etc. As such, the method is most helpful in grassroots or regional mineral exploration contexts, but could also be used to evaluate alterations quantified using other methods, and is thus viewed as complementary of existing methods.

Computer code

The method presented in this contribution is provided as a computer code (C++ language).

Acknowledgements

The authors wish to address special thanks to the editor and reviewers of the manuscript, Jef Caers and David Lentz, as well as an anonymous reviewer. This project was supported by Canada Economic Development, the Ministère de l'Énergie et des Ressources Naturelles du Québec, the Conférence Régionale des élus Saguenay-Lac-Saint-Jean and companies members of the Consorem. The authors warmly thank their colleague Silvain Rafini for constructive discussions on this project, Geneviève Boudrias for editing the original Consorem report on this work (report available online at http://www.consorem.ca/), Judit Ozoray for correcting this manuscript's spelling and the various users of the non-public LithoModeleur software, that integrates the method presented here since April 2008.

Appendix A. Supplementary material

Supplementary data associated with this article can be found in the online version at http://dx.doi.org/10.1016/j.cageo.2016.01.003.

References

Bédard, J.H., 2006. A catalytic delamination-driven model for coupled genesis of Archaean crust and sub-continental lithospheric mantle. Geochim. Cosmochim. Acta 70 (5), 1188–1214.

Barrett, T.J., MacLean, W.H., 1994. Chemostratigraphy and hydrothermal alteration in exploration for VHMS deposits in greenstones and younger volcanic rocks. In: Lentz, D.R. (Ed.), Alteration and Alteration Processes Associated with Ore-forming Systems 11. Geological Association of Canada, Canada, pp. 433–465, short course notes.

Boari, E., Tommasini, S., Laurenzi, M.A., Conticelli, S., 2009. Transition from ultrapotassic kamafugitic to sub-alkaline magmas: Sr, Nd and Pb isotope, trace element and ^{40}Ar–^{39}Ar Age data from the Middle Latin Valley Volcanic Field, Roman Magmatic Province, Central Italy. J. Petrol. 50, 1327–1357.

Cadieux, A.-M., Dubé, B., Williamson, K., Malo, M., Twomey, T., 2006. Characterization of hydrothermal alterations at the Red Lake mine, northwestern Ontario. Geological Survey of Canada, Current Research 2006-C2, 14p.

Cann, J.R., 1970. Rb, Sr, Y, Zr and Nb in some ocean-floor basaltic rocks. Earth Planet. Sci. Lett. 10 (1), 7–11.

Cohen, J.F., 2011. Mineralogy and Geochemistry of Hydrothermal Alteration at the Ann- Mason Porphyry Copper Deposit, Nevada: Comparison of Large-scale Ore Exploration Techniques to Mineral Chemistry (Unpublished Master Thesis). Oregon State University, United States, p. 580.

Cohen, J.F., Dilles, J.H., Tosdal, R.M., Halley, S., 2011. Compositional variations in hydrothermal white micas and chlorites in a porphyry Cu system at Yerington. Abstracts with Programs – Geological Society of America, May, vol. 43, 4, pp. 63–64.

Dilles, J.H., 2012. Footprints of Porphyry Cu Deposits: Vectors to the Hydrothermal Center Using Mineral Mapping and Lithogeochemistry p. 599, Technical Report for USGS MRERP Grant Award number G10AP00052.

Drummond, M.S., Defant, M.J., 1990. A model for trondhjemite-tonalite-dacite genesis and crustal growth via slab melting: Archean to modern comparisons, J. Geophys. Res-Sol. Ea., 95 (B13), 21503–21521.

Finlow-Bates, T., Stumpfl, E.F., 1981. The behaviour of so-called immobile elements in hydrothermally altered rocks associated with volcanogenic submarine exhalative ore deposits. Miner. Deposita 16, 319–328.

GEOROC – Geochemistry of Rocks of the Oceans and Continents, 2011. Max-Planck-Institut für Chemie. ⟨http://georoc.mpch-mainz.gwdg.de/georoc/Start.asp⟩ (accessed 30.11.11).

Grant, J.A., 1986. The Isocon Diagram – a simple solution to gresens's rquation for metasomatic alteration. Econ. Geol. 81, 1976–1982.

Grant, J.A., 2005. Isocon analysis: a brief review of the method and applications. Phys. Chem. Earth Parts A/B/C 30 (17), 997–1004.

Gresens, R.L., 1967. Composition–volume relationships of metasomatism. Chem. Geol. 2, 47–55.

Hastie, A.R., Kerr, A.C., Pearce, J.A., Mitchell, S.F., 2007. Classification of altered volcanic island arc rocks using immobile trace elements: development of the Th–Co discrimination diagram. J. Petrol. 48 (12), 2341–2357.

Hill, I.G., Worden, R.H., Meighan, I.G., 2000. Yttrium: the immobility–mobility transition during basaltic weathering. Geology 28, 923–926.

Hornik, K., Stinchcombe, M., White, H., 1989. Multilayer feedforward networks are universal approximators. Neural Netw. 4, 251–257.

Hughes, C.J., 1972. Spilites, keratophyres and the igneous spectrum. Geol. Mag. 109, 515–527.

Hynes, A., 1980. Carbonitization and mobility of Ti, Y, and Zr in Ascot formation metabasalts, S.E. Quebec. Contrib. Mineral. Petrol. 75, 79–87.

Jiang, S.-Y., Wang, R.-C., Xu, X.-S., Zhao, K.-D., 2005. Mobility of high field strength elements (HFSE) in magmatic-, metamorphic-, and submarine-hydrothermal systems. Phys. Chem. Earth 30, 1020–1029.

Kurtz, A.C., Derry, L.A., Chadwick, O.A., Alfano, M.J., 2000. Refractory element mobility in volcanic soils. Geology 28, 683–686.

Le Maitre, R.W., Bateman, P., Dudek, A., Keller, J., Lameyre, J., Le Bas, M.J., Sabine, P. A., Schmid, R., Sorensen, H., Streckeisen, A., Woolley, A.R., Zanettin, B., 1989. A Classification of Igneous Rocks and Glossary of Terms: Recommendations of the International Union of Geological Sciences Subcommission on the Systematics of Igneous Rocks. Blackwell Scientific Publications, Oxford, p. 206.

Le Bas, M.J., Le Maitre, R.W., Streckeisen, A., Zanettin, B., 1986. A chemical classification of volcanic rocks based on the total alkali-silica diagram. J. Petrol. 27, 745–750.

Leitch, C.H.B., Lentz, D.R., 1994. The Gresens approach to mass balance constraints of alteration systems: methods, pitfall, examples. Alteration and Alteration Processses Associated with Ore-forming Systems 11. Geological Association of Canada, Canada, pp. 161–192, short course notes.

MacLean, W.H., Kranidiotis, P., 1987. Immobile elements as monitors of mass transfer in hydrothermal alteration: Phelps Dodge massive sulphide deposit, Matagami, Québec. Econ. Geol. 82, 951–962.

Mattsson, H.B., Oskarsson, N., 2005. Petrogenesis of alkaline basalts at the tip of a propagating rift: evidence from the Heimaey volcanic centre, south Iceland. J. Volcanol. Geotherm. Res. 147, 245–267.

McCulloch, M.T., Gamble, J.A., 1991. Geochemical and geodynamical constraints on subduction zone magmatism. Earth Planet. Sci. Lett. 102, 358–374.

Meschede, M., 1986. A method of discriminating between different types of mid-ocean ridge basalts and continental tholeiites with the Nb–Zr–Y diagram. Chem. Geol. 56 (3), 207–218.

Nesbitt, H.W., 2003. Petrogenesis of siliciclastic sediments and sedimentary rocks. In: Lentz, D.R. (Ed.), Geochemistry of Sediments and Sedimentary Rocks: Evolutionary Considerations to Mineral Deposits-forming Environments. Geological Association of Canada, Canada, pp. 39–51, GeoText 4.

NeuroDimension, 2012. NeuroSolutions for Excel 6.11. ⟨http://www.neurosolutions.com/⟩ (accessed 20.06.12).

Pallister, J.S., Thornber, C.R., Cashman, K.V., Clynne, M.A., Lowers, H.A., Mandeville, C.W., Brownfield, I.K., Meeker, G.P., 2008. Petrology of the 2004–2006 Mount St. Helens lava dome – Implications for magmatic plumbing and eruption triggering. In: Sherrod, D.R., Scott, W.E., Stauffer P.H. (Eds.), A volcano rekindled: the renewed eruption of Mount St. Helens, 2004–2006. U.S. Geological Survey Professional Paper 1750, pp. 647–702.

Pearce, J.A., 1996. A user's guide to basalt discrimination diagrams. Trace Element Geochemistry of Volcanic Rocks: Applications for Massive Sulphide Exploration 12. Geological Association of Canada, Canada, pp. 79–113, short course notes 12.

Pearce, J.A., 2008. Geochemical fingerprinting of oceanic basalts with applications to ophiolite classification and the search for Archean oceanic crust. Lithosphere 100 (1), 14–48.

Pearce, J.A., Cann, J.R., 1973. Tectonic setting of basic volcanic rocks determined using trace element analyses. Earth Planet. Sci. Lett. 19, 290–300.

Pearce, J.A., Norry, M.J., 1979. Petrogenetic implications of Ti, Zr, Y, and Nb variations in volcanic rocks. Contrib. Mineral. Petrol. 69 (1), 33–47.

Pearce, T.H., 1968. A contribution to the theory of variation diagrams. Contrib. Mineral. Petrol. 19 (2), 142–157.

Petford, N., Atherton, M., 1996. Na-rich partial melts from newly underplated basaltic crust: the Cordillera Blanca Batholith, Peru. J. Petrol. 37 (6), 1491–1521.

Relvas, J.M., Barriga, F.J., Ferreira, A., Noiva, P.C., Pacheco, N., Barriga, G., 2006. Hydrothermal alteration and mineralization in the Neves-Corvo volcanic-hosted massive sulfide deposit, Portugal. I. Geology, mineralogy, and geochemistry. Econ. Geol. 101 (4), 753–790.

Ross, P.S., Bédard, J.H., 2009. Magmatic affinity of modern and ancient subalkaline volcanic rocks determined from trace-element discriminant diagrams. Can. J. Earth Sci. 46 (11), 823–839.

Salvi, S., Fontan, F., Monchoux, O., Williams-Jones, A.E., Moine, B., 2000. Hydrothermal mobilization of high field strength elements in alkaline igneous systems: evidence from the Tamazeght Complex (Morocco). Econ. Geol. 95, 559–576.

Sarbas, B., 2008. The GEOROC database as part of a growing geoinformatics network. In: Brady, S.R., Sinha, A.K., Gundersen, L.C. (Eds.), Geoinformatics 2008, Data to Knowledge, Proceedings. U.S. Geological Survey Scientific Investigations Report 2008-5172, pp. 42–43.

Schandl, E.S., Gorton, M.P., 2002. Application of high field strength elements to discriminate tectonic settings in VMS environments. Econ. Geol. 97 (3), 629–642.

Schiano, P., Dupré, B., Lewin, E., 1993. Application of element concentration variability to the study of basalt alteration (Fangataufa atoll, French Polynesia). Chem. Geol. 104 (1), 99–124.

Shriver, N.A., MacLean, W.H., 1993. Mass, volume and chemical changes in the alteration zone at the Norbec mine, Noranda, Québec. Miner. Deposita 28, 157–166.

Stanley, C.R., Madeisky, H.E., 1994. Lithogeochemical exploration for hydrothermal ore deposits using Pearce element ratio analysis: Alteration and alteration processes associated with ore forming systems. Geological Association of Canada Short Course Notes 11, pp. 193–211.

Stanley, C.R., Russell, J.K., 1989. Petrologic hypothesis testing with Pearce element ratio diagrams: derivation of diagram axes. Contrib. Mineral. Petr., 103 (1), 78–89.

Trépanier, S., Mathieu, L., Daigneault, R., 2015. CONSONORM_LG: new normative minerals and alteration indexes for low-grade metamorphic rocks. Econ. Geol., http://dx.doi.org/10.2113/econgeo.110.8.2127

Van Dongen, M., Weinberg, R.F., Tomkins, A.G., 2010. REE-Y, TI, and P remobilization in magmatic rocks by hydrothermal alteration during Cu–Au deposit formation. Econ. Geol. 105 (4), 763–776.

Wang, C., Venkatesh, S.S., Judd, J.S., 1994. Optimal stopping and effective machine complexity in learning. In: Cowan, J.D., Tesauro, G., Alspector J. (Eds.), Advances in Neural Information Processing Systems, Morgan Kaufmann, San Francisco, pp. 303–310. (Denver, 1993).

Winchester, J.A., Floyd, P.A., 1977. Geochemical discrimination of magma series and their differentiation products using immobile elements. Chem. Geol. 20, 325–343.

Wood, D.A., 1980. The application of a Th-Hf-Ta diagram to problems of tectono-magmatic classification and to establishing the nature of crustal contamination of basaltic lavas of the British Tertiary Volcanic Province. Earth Planet. Sci. Lett. 50 (1), 11–30.

Zurada, J.M., 1992. Introduction to Artificial Neural Systems. West Publishing Company, St. Paul, Minnesota, p. 758.